Visualization of Shoulder Range of Motion for Clinical Diagnostics and Device Development

Arno H.A. Stienen*†‡ and Arvid Q.L. Keemink*‡
* Biomechanical Engineering, University of Twente, Enschede (NL).
† Physical Therapy and Human Movement Sciences, Northwestern University, Chicago (USA).
‡Both authors contributed equally to this work. Email: arnostienen@gmail.com.

***Abstract*—Rotations of the humerus in the human shoulder girdle are usually described using five classical medical definitions: flexion/extension, abduction/adduction, internal/external rotation, horizontal abduction/adduction, and horizontal flexion/extension. The latter two are needed to overcome the inability of the first three to define the full range of motion. The International Society for Biomechanics recommendations reduce these to three sequential rotations around perpendicular axes: rotation of the plane of elevation (horizontal rotation), elevation, and axial rotation. We expand on this work by providing a new and intuitive visualization method to display these rotations that superimposes the axial rotation on the map projection of the reachable workspace of the elbow. We provide methods to interpret and create the visualization using direct observations, but also the equations and Matlab scripts needed to use the method. The visualization allows the immediate observation of the full rotational range of motion of the humerus and the interaction effects between these physiologically coupled rotations. Furthermore, it allows visualization of the effects of kinematic limitations of external devices such as endpoint manipulators or exoskeletons. Therefore, the new visualization method is useful for both clinical diagnostics and device development.**

I. Introduction

In this work we present a novel and intuitive visualization method for displaying the kinematics of the glenohumeral (GH) rotations of the human shoulder girdle. The visualization method displays the rotations of the girdle via superposition of the axial rotation on the map projection of the reachable workspace of the elbow. An example of the visualization is given in Fig. 1.

The human shoulder girdle is a complex skeletal structure with a remarkably large range of motion (ROM). Many have measured the GH rotations [1]–[3], using a selection of the five classical movement directions: flexion/extension, abduction/adduction, internal/external rotation, horizontal abduction/adduction, and horizontal flexion/extension (see Fig. 2). These classical movements are conceptually easy to under-

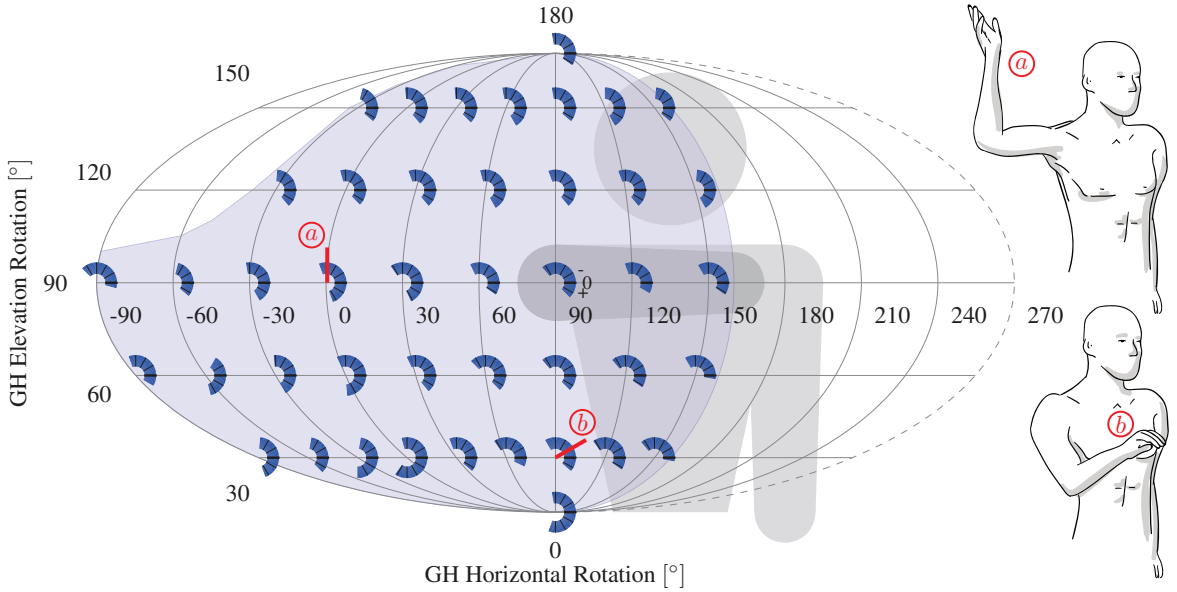

Fig. 1. Visualization example of the measured rotational range of motion of the right humerus of a single subject. The sphere of the workspace of the elbow, as defined by the glenohumeral (GH) horizontal and elevation rotations alone, is flattened using the Mollweide map projection. The projection is viewed from an external observer looking at the subject. The GH axial rotations are shown as arcs at discrete grid-points, with each arc representing the reachable movement of the forearm with an (imaginary) flexed elbow at 90°, as seen from the observer when looking through the respective grid point at the GH rotation center. The shaded background area shows the reachable angles in GH horizontal and elevation rotation. Right: two examples of arm orientations (ⓐ and ⓑ) mapped to the corresponding location and orientation the map projection.

978-1-4799-1808-9/15/$31.00

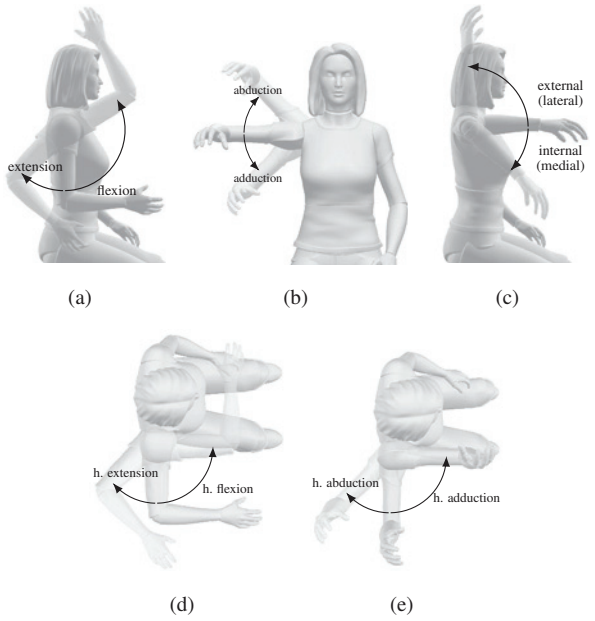

Fig. 2. The five classical definitions of movement directions for three degrees of freedom of the shoulder: a) flexion/extension, b) abduction/adduction, c) internal/external rotation, d) horizontal flexion/extension, and e) horizontal abduction/adduction.

stand, but the inclusion of the latter two is needed to overcome the inability of the first three to define the full range of motion. Furthermore, the rotations are defined around an immovable global joint coordinate system that makes sequential rotations around multiple of the defined axes prone to interpretation differences. To solve these problems, the International Society for Biomechanics (ISB) recommendations reduce these five classical rotations to three sequential rotations around perpendicular axes [4]: GH rotation of the plane of elevation, GH elevation (negative), and GH axial rotation[1]. In this paper we will use the ISB definitions but refer to them as GH horizontal rotation, GH elevation rotation, and GH axial rotation for brevity and clarity.

Independent of the joint coordinate system used, nearly all studies that report on the GH ROM give the measurements for each axis as an independent outcome measure. This ignores the interaction effects between these physiologically coupled rotations and leads to a reported ROM that is likely larger than actually achievable. This might especially affect reporting in clinical diagnostics, which require the ROM to be measured and represented properly.

External interaction with the shoulder girdle is possible with a wide variety of devices, from endpoint manipulators and weight-support devices to exoskeletons and orthotics. Of these, exoskeletons are often used to directly augment the three rotations of the GH joint [5]–[8]. Again, common presentations of human shoulder or exoskeleton shoulder ROM results are tables or graphs that indicate by numerical intervals or plotted bars the ROM along the movement directions [1], [9]–[15], under the assumption that these movement ranges are decoupled. In [5], [6], [16], [17] a more graphical approach is taken. They visualized the range of motion by creating a 3D point cloud around the human body, indicating the reachable workspace of the human arm. The third rotation, GH axial rotation, is not represented in these point clouds. The globe system [18] recognizes that a sphere of elbow positions around the humeral head is fully defined by GH horizontal and elevation rotations. It gives the same angle definitions as the ISB recommendations to decompose arm rotations onto this sphere. The axial rotation component is mainly neglected, or drawn on a front or top view of the sphere. In publication, it presents only single arm configurations using multiple top and side views, and gives therefore no information about shoulder ROM. All these presentation methods have in common that they are often hard to interpret due unintuitive representations or by attempting to show 3D objects in 2D print.

We have therefore built upon the aforementioned work an developed a new visualization method to show the complete shoulder ROM[2]. Our method uses a single figure to show complete range of motion in 2D print. With this method we can inspect functional ROM of patients, compare the human shoulder ROM to an exoskeleton shoulder ROM, or compare different exoskeleton shoulders. Furthermore, we will use this visualization to show kinematic or dynamic properties of exoskeleton shoulder joints.

II. Background

A. Kinematics of the Human Shoulder

To geometrically describe the human shoulder, we use axes and angles definitions from the ISB [4]. As shown in Fig. 3, a global coordinate frame is attached to the center of rotation in the glenohumeral (GH) rotation center of the shoulder. The global $\mathbf{x}$-axis points in the dorsoventral direction (forward), the global $\mathbf{y}$-axis points in the anteroposterior direction (upward) and the global $\mathbf{z}$-axis points into the mediolateral direction (outward to the right).

The human shoulder orientation is decomposed around these axes into YXY intrinsic Euler angle rotations. These rotations are stated in the order of most to least dominant rotation, i.e. a dominant rotation also rotates a less dominant axis. Classically this YXY decomposition would be (dominant) Y: horizontal abduction/adduction, X: abduction/adduction, and (least dominant) Y: internal/external rotation.

The shoulder rotates a person's upper arm, which makes the tip of the elbow cover part of the surface of a sphere (i.e. the 'elbow-tip sphere'). This sphere can be decomposed into spherical coordinates: the GH horizontal rotation γ_h and GH elevation rotation γ_e (the first two most dominant YX

[1]As in [4], the methods presented here are valid for the right shoulder only. Whenever left shoulders are measured, it is recommended to mirror the raw position data with respect to the sagittal plane. Finally, this paper focuses on the GH rotations only and ignores any translations of the GH rotation center.

[2]An animation explaining the method, and Matlab macro code to represent your design or measurement data with our method can be found at `http://ctw-bw124.ctw.utwente.nl:9988/ShROMVis`

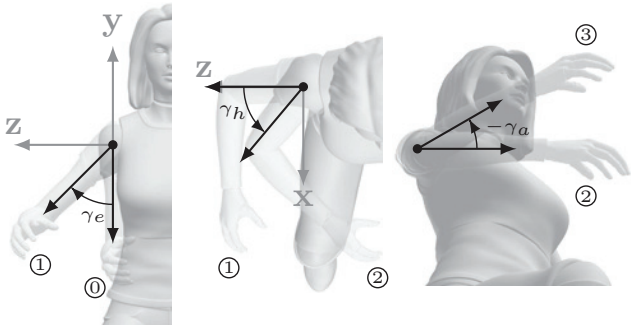

Fig. 3. ISB Axes definitions, $\mathbf{x}$ pointing forward, $\mathbf{y}$ pointing upward and $\mathbf{z}$ pointing outward. Intuitive ISB angle decomposition from left to right; Front view: GH elevation rotation first (from pose ⓪ to ①, over angle γ_e). Top view: rotate horizontally (from pose ① to ②, over angle γ_h). View perpendicular to the upper arm: finally, rotate axially (from pose ② to ③, over angle γ_a).

rotations). The third and least dominant upper arm rotation, GH axial rotation, is described directly by γ_a, relative to the horizontal plane. Positive GH elevation rotation is defined as a clockwise rotation in the rotated elevation plane around the rotated $\mathbf{x}$-axis. The GH horizontal rotation is defined as counter-clockwise around the global $\mathbf{y}$-axis, with 0° GH horizontal rotation making the GH elevation rotation pure shoulder ab-/adduction, and 90° GH horizontal rotation making GH elevation rotation pure shoulder flexion/extension. The GH axial rotation is defined as being positive in clockwise direction (i.e. positive for internal/lateral rotation) around the upper arm vector (not common for right handed coordinate systems).

This decomposition is intuitively understood when performed by a person in a different order than the geometrical description, due to the singular nature of the YXY rotation order (i.e. the unresolvable ambiguity between horizontal and axial rotation in some orientations). The decomposition is shown in Fig. 3 and described as follows:

1) First, a person elevates the arm from the zero-configuration (rotation from orientation ⓪ to ① over angle γ_e)
2) Secondly, the person performs horizontal rotation (rotation from orientation ① to ②, over angle γ_h).
3) Finally, the person rotates axially (rotation from orientation ② to ③, over angle γ_a.

Our initial- or zero-configuration is defined as the one with the upper arm pointing vertically down (orientation ⓪ in Fig. 3). In the zero-configuration the elbow is touching a person's side. For ease of reasoning, and to avoid ambiguity, we always assume 90° elbow flexion.

B. Kinematics of the Exoskeleton Shoulder

For any exoskeleton shoulder we will use the same global axes as for the human shoulder (Sec. II-A). Generically, a shoulder exoskeleton is regarded as a series of three sequential rotations. Although parallel exoskeleton shoulder actuation do exist [11]. In this work we will compare several exoskeleton shoulder design configurations conceptually in Sec. IV.

TABLE I
JOINT ZERO-CONFIGURATIONS OF EXOSKELETON SHOULDER DESIGNS. *ROTATED Z, **FIRST AXIS $< 45^\circ$ ROTATED AWAY FROM PRINCIPAL, BAR IMPLIES NEGATIVE DIRECTION.

Order	**Name** [7], [8]
YZY	ArmeoPower, ArmeoSpring, ARMIN (chARMin, I-IV), Dampace, ExoRob, FREFLEX, IntelliArm, Limpact, (pneu-)WREX*, SUEFUL-7
$\bar{X}YZ$	ABLE, BONES
$\bar{X}ZY$	L-Exos, CADEN-7**, RehabExos**, Salford ARE$^{(*)}$
$Y\bar{X}Z$	MEDARM**, MGA**, MULOS*

The order of rotations in the human's zero configuration we will call the exoskeleton's *rotation order*. If the rotation order is for instance XYZ, this implies that the first (*most dominant*) rotation axis is the global $\mathbf{x}$-axis, the second rotation axis is the global $\mathbf{y}$-axis and the third (*least dominant*) rotation axis is the global $\mathbf{z}$-axis. Note that these axes only coincide with the global axes in the human's zero orientation, and the second and third axes will be rotated away from the principal axes by moving the human arm.

Common rotation orders are the orthogonal designs (a bar denoting negative direction): YZY, $\bar{X}YZ$, $\bar{X}ZY$ and $Y\bar{X}Z$. Also, several designs place the first rotation axis in none of the principal directions [10], [19], [20] and do not necessarily have the same kinematic properties as the four major orders. A list of several common designs is shown in Table I. Useful references to these designs can be found in [7] and [8].

III. METHOD

A. Shoulder ROM Projection

We choose the Mollweide (or homolographic) projection [21] to expand a spherical surface onto a 2D plane. The Mollweide projection is preferred to an equirectangular projection (in which points of GH elevation and GH horizontal rotations form a *rectangular* grid), due to the equirectangular projection's ambiguity at the poles and the Mollweide projection's aesthetic properties.

We place the 90° GH elevation rotation and 90° GH horizontal rotation in the center of the map, as is shown by a gray human figurine in the background of the figure holding its arm in $\gamma_h = 90^\circ$, $\gamma_e = 90^\circ$, $\gamma_a = 0^\circ$ orientation. This changes the map range from 0° to 180° in GH elevation rotation and -90° to 270° in GH horizontal rotation, compared to conventional world maps in longitude and latitude. The $+270^\circ$ meridian is equivalent to the -90° meridian, and is therefore *never* used and shown as a dashed line. Equations to calculate the projection can be found in the Appendix.

In addition, we can also show the complete GH horizontal and elevation bounds by using a half-transparent shaded area,

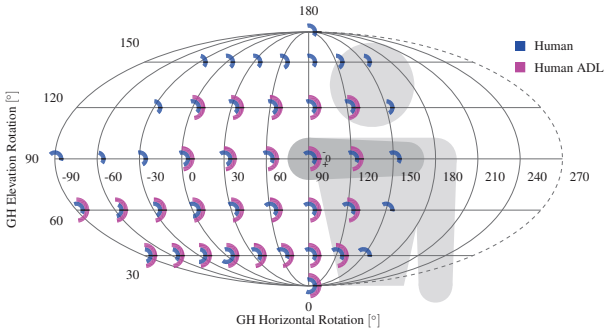

Fig. 4. Measured ROM of the subject compared to specified ROM ADL-movements as measured in [3].

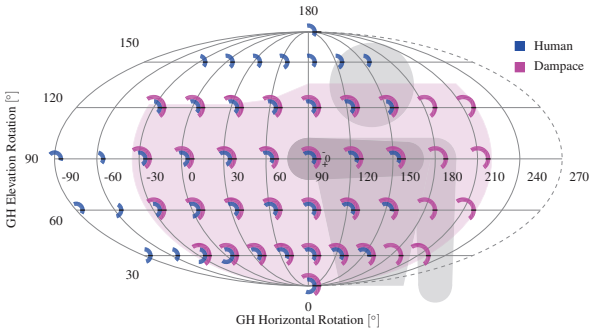

Fig. 5. Real movement range of the Dampace [9], including joint limits, internal collisions and body collisions, compared to the human shoulder ROM.

as is done in Fig. 1 and Fig. 5. This area is most of the time left out if it is irrelevant, and to limit the amount of information presented to the reader.

B. Showing Axial Rotations

The GH axial rotation ROM of the shoulder is shown on the Mollweide-grid on *discrete locations*. Discrete intervals are usable since the axial ROM varies rather smoothly over the complete sphere of GH horizontal and elevation rotation. The axial ROM is shown as an arc. Counter-clockwise rotation is negative axial rotation (i.e. external rotation), clockwise is positive axial rotation (i.e. internal rotation). Notice the small 0, $-$ and $+$ sign at the $90°$ elevation pose of the figurine in the background in Fig. 1. In this work we space these arcs on intervals $30°$ apart in horizontal and elevation rotation, although greater and smaller intervals are possible. If only a single axial orientation is shown (instead of a range), a thicker single line (like a clock hand) is shown, as is done in Fig. 1 for two example arm orientations.

C. Measurement Method

To measure the ROM of the shoulder we propose the following method to be performed for reachable chosen grid-points (a visual representation of the method is given in Fig. 3). This might not be an optimal way to determine the shoulder ROM, but we would like to emphasize that the visualization and *not* the measurement method is of main interest in this work. The method used to generate results in Sec. IV is as follows:

1) The subject is placed in the initial-configuration ($\gamma_h = 0°$,$\gamma_e = 0°$,$\gamma_a = 0°$) with the upper arm pointing down, and the forearm pointing forward ($90°$ elbow flexion).
2) The subject performs GH elevation rotation (γ_e) of the arm, away from the zero-configuration.
3) The subject performs GH horizontal rotation (γ_h). At the end of this motion, the forearm should be horizontal.
4) The subject performs GH axial rotation (γ_h) to the extremes in both directions. These extremes give the complete range of axial rotation at this grid-point, and these have to be recorded.

The orientation can be recorded and confirmed through a (digital) goniometer, or through an (inertial) motion tracking system. If the subject cannot move his or her own arm, a physician has to perform the aforementioned steps.

To display properties of exoskeleton designs, the same protocol can be followed.

IV. Example Cases

The power of the method is demonstrated by using it for several examples of different design and presentation goals: 1) showing ROM measurement data of a subject, compared to an ADL measurement, 2) showing the limited ROM of an existing exoskeleton design when explained by classical movement ranges, 3) showing kinematic exoskeleton design properties in terms of kinematic conditioning, 4) showing the complexity of the design problem of choosing mechanical joint limits for exoskeleton design.

The method was used to determine the human ROM (a healthy male subject, 19 y.o.), shown in Fig. 4. The subject was measured using a goniometer. Coupling is observed between the GH horizontal and GH elevation rotation and the range of GH axial rotation. The ROM is compared to the one measured in [3] for ADL movements to show that moving along the classical directions shows a different determined ROM without coupling effects. It cannot be ruled out that the different size of ROM is due to the subject(s) or the method.

We show in Fig. 5 the measured ROM of the passive Dampace Exoskeleton [9], including the complete GH horizontal and elevation region in the shaded area. We compare the measured range with the human one, to show how well the exoskeleton supports the human ROM.

Next, we show the kinematic conditioning of three main exoskeleton shoulder types YZY, $\bar{X}YZ$ and $\bar{X}ZY$ in Fig. 6. The exoskeleton conditioning is calculated by taking the absolute determinant of only the square rotation Jacobian of the system. The conditioning ranges therefore in value from 0 to 1. The figures directly show the benefits of several rotation orders for a specified task ROM. It also shows that some rotation orders, such as $\bar{X}ZY$ are better avoided. Therefore in [10] they actually placed the first axis under a $45°$ angle,

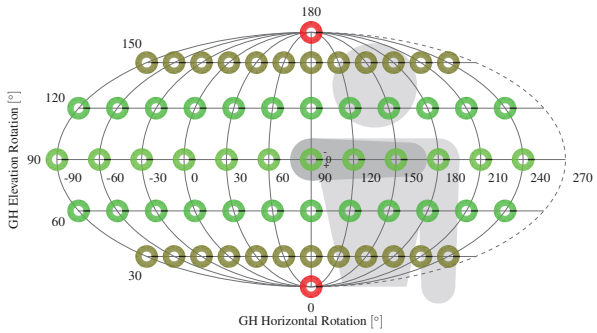

(a) YZY

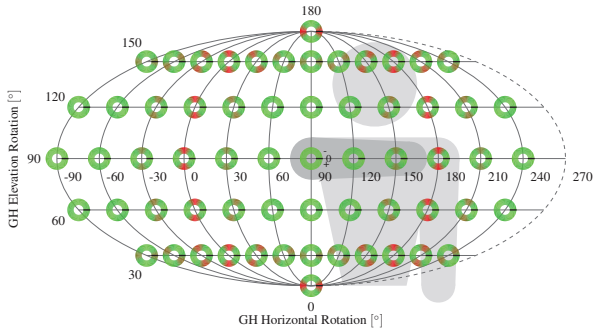

(b) $\bar{X}YZ$

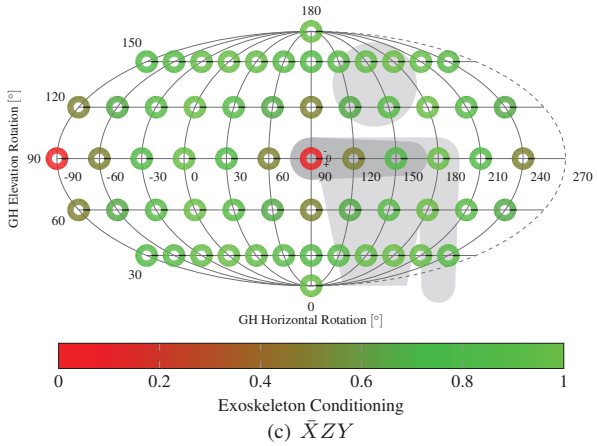

(c) $\bar{X}ZY$

Fig. 6. Illustration of conditioning of three common rotation orders: a) YZY b) $\bar{X}YZ$ c) $\bar{X}ZY$. Joint conditioning is shown as a red-to-green gradient (red = gimbal lock, green = perfect conditioning).

moving the singularity towards higher GH horizontal rotation angle.

Finally, we use the measurement data to show extreme choices of mechanically limiting rotations for YZY and $Y\bar{X}Y$ rotation orders (or for inverted versions of the rotation axes). If the minimal rotation ranges are picked, as in Fig. 7(a), the design is very safe, but very conservative and unusable. If the maximal rotation ranges are picked, as in Fig. 7(b), the human achieves full range of motion, but the exoskeleton cannot be inherently mechanically safe and needs angle limitations in software.

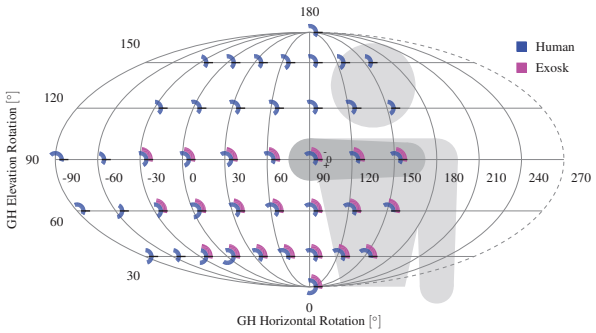

(a)

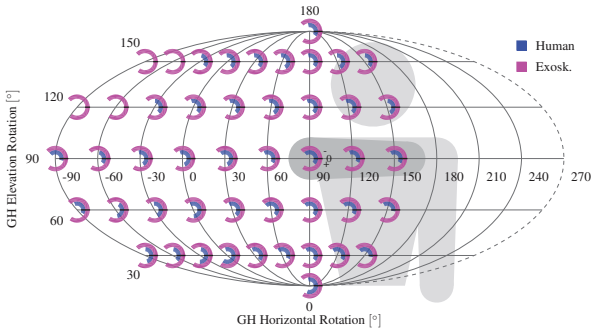

(b)

Fig. 7. Implications of choosing mechanical joint limits in exoskeletons. a) All rotations of the exoskeleton limited to the minimum range b) All rotations of the exoskeleton limited to the maximum range. Both figures are only valid for YZY or $Y\bar{X}Y$.

V. Discussion

The visualization method can be used to display a large variety of useful information about standard human shoulder ROM, pathological ROM, ADL ROM, assistive device ROM and mechanical, kinematic or dynamic device properties.

Compared to presentation of classical movement ranges of the human shoulder in tables, this method does take more publication space, but gives a more complete picture. The addition of our method to the globe system [18] is the possibility to show complete ROM directly, including axial rotation, without using different camera viewpoints. Compared to plotting 3D points or a surface in a 2D image, our method is clear and less ambiguous, also directly including GH axial rotations.

Using our method to display device ROM is useful if its ROM is compared to the human ROM and show its dynamic or kinematic properties over the *human* workspace. For a separate robotic device the joint limits could already be sufficient to determine their own complete ROM.

The given examples demonstrate that for a select set of challenges, the extended effort needed to acquire the full set of measurements needed for the visualization are worth the effort in collection.

A minor drawback, due to the ISB decomposition of rotation into three Euler angles, is the representation singularity in the arm's zero-configuration. A shoulder flexion to hyper-

extension motion with the forearm forward would imply an instantaneous 180° jump in GH horizontal (from $+90^\circ$ to -90°) *and* GH axial rotation (from $+90^\circ$ to -90°). This jump in angles is counter-intuitive.

Future work will include simplifying the required data collection, using inertial measurement systems. Measuring more subjects will help introducing a statistical certainty measure of the achieved ROM, which can be included in the visualization. Finally, this method will be evaluated with clinicians, industrial partners to show its usefulness in displaying progression of shoulder rehabilitation and the benefit of assistive and rehabilitation devices.

Appendix: The Mollweide Projection

To preserve scaling in plotting applications, the extremes of the Mollweide projection (the poles and the lateral 'sides') are mapped onto to the range: $y \in [0^\circ, 180^\circ]$, $x \in [-90^\circ, 270^\circ)$. These four extremes are then mapped to the same points as for an equirectangular projection. This scaling is preserved if the following is used to calculate the projected spherical coordinates γ_h and γ_e (given in degrees) onto a 2D plane:

$$x = R\frac{2\sqrt{2}}{\pi}\cos(\theta)\frac{(\gamma_h - 90^\circ)\pi}{180^\circ} + 90^\circ$$
$$y = R\sqrt{2}\sin(\theta) + 90^\circ,\ R = \frac{90^\circ}{\sqrt{2}}$$

with the implicit equation

$$\theta = \frac{\pi\sin(\gamma_e - 90^\circ) - \sin(2\theta)}{2}. \quad (1)$$

Note in (1) that γ_e is entered in degrees ($[^\circ]$). Care has to be taken in software applications by possibly converting the value to radians for a proper $\sin(\cdot)$ argument.

Eq. (1) can be solved by Newton-Raphson iteration [21]:

$$\theta_{n+1} = \theta_n - \frac{2\theta_n + \sin(2\theta_n) - \pi\sin(\gamma_e - 90^\circ)}{2 + 2\cos(2\theta_n)},$$

which has to be repeated until convergence and will give a value in radians.

Acknowledgment

The authors would like to thank Floris M. Bloembergen and Anke Nesselaar for their support. This research is supported by the Dutch Technology Foundation STW, which is part of the Netherlands Organisation for Scientific Research (NWO), and which is partly funded by the Ministry of Economic Affairs. Project Number: 12162.

References

[1] C. J. Barnes, S. J. Van Steyn, and R. A. Fischer, "The effects of age, sex, and shoulder dominance on range of motion of the shoulder," *Journal of Shoulder and Elbow Surgery*, vol. 10, no. 3, pp. 242–246, 2001.

[2] K. Hayes, J. R. Walton, Z. L. Szomor, and G. A. Murrell, "Reliability of five methods for assessing shoulder range of motion," *Australian Journal of Physiotherapy*, vol. 47, no. 4, pp. 289–294, 2001.

[3] S. Namdari, G. Yagnik, D. D. Ebaugh, S. Nagda, M. L. Ramsey, G. R. Williams, and S. Mehta, "Defining functional shoulder range of motion for activities of daily living," *Journal of shoulder and elbow surgery*, vol. 21, no. 9, pp. 1177–1183, 2012.

[4] G. Wu, F. C. Van Der Helm, H. D. Veeger, M. Makhsous, P. Van Roy, C. Anglin, J. Nagels, A. R. Karduna, K. McQuade, X. Wang *et al.*, "ISB recommendation on definitions of joint coordinate systems of various joints for the reporting of human joint motion–Part II: shoulder, elbow, wrist and hand," *Journal of biomechanics*, vol. 38, no. 5, pp. 981–992, 2005.

[5] A. Schiele and F. C. van der Helm, "Kinematic design to improve ergonomics in human machine interaction," *Neural Systems and Rehabilitation Engineering, IEEE Transactions on*, vol. 14, no. 4, pp. 456–469, 2006.

[6] P. Letier, M. Avraam, S. Veillerette, M. Horodinca, M. De Bartolomei, A. Schiele, and A. Preumont, "SAM : A 7-DOF portable arm exoskeleton with local joint control," in *Intelligent Robots and Systems, 2008. IROS 2008. IEEE/RSJ International Conference on*, Sept 2008, pp. 3501–3506.

[7] H. S. Lo and S. Q. Xie, "Exoskeleton robots for upper-limb rehabilitation: State of the art and future prospects," *Medical engineering & physics*, vol. 34, no. 3, pp. 261–268, April 2012.

[8] P. Maciejasz, J. Eschweiler, K. Gerlach-Hahn, A. Jansen-Troy, S. Leonhardt *et al.*, "A survey on robotic devices for upper limb rehabilitation," *Journal of neuroengineering and rehabilitation*, vol. 11, no. 3, January 2014.

[9] A. H. Stienen, E. E. Hekman, F. C. Van der Helm, G. B. Prange, M. J. Jannink, A. M. Aalsma, and H. Van der Kooij, "Dampace: dynamic force-coordination trainer for the upper extremities," in *Rehabilitation Robotics, 2007. ICORR 2007. IEEE 10th International Conference on*. IEEE, 2007, pp. 820–826.

[10] J. C. Perry, J. Rosen, and S. Burns, "Upper-limb powered exoskeleton design," *Mechatronics, IEEE/ASME Transactions on*, vol. 12, no. 4, pp. 408–417, 2007.

[11] J. Klein, S. Spencer, J. Allington, K. Minakata, E. Wolbrecht, R. Smith, J. Bobrow, and D. Reinkensmeyer, "Biomimetic orthosis for the neurorehabilitation of the elbow and shoulder (BONES)," in *Biomedical Robotics and Biomechatronics, 2008. BioRob 2008. 2nd IEEE RAS & EMBS International Conference on*. IEEE, 2008, pp. 535–541.

[12] H.-S. Park, Y. Ren, and L.-Q. Zhang, "IntelliArm: an exoskeleton for diagnosis and treatment of patients with neurological impairments," in *Biomedical Robotics and Biomechatronics, 2008. BioRob 2008. 2nd IEEE RAS & EMBS International Conference on*. IEEE, 2008, pp. 109–114.

[13] T. Nef, M. Guidali, and R. Riener, "ARMin III–arm therapy exoskeleton with an ergonomic shoulder actuation," *Applied Bionics and Biomechanics*, vol. 6, no. 2, pp. 127–142, 2009.

[14] M. J. Mullaney, M. P. McHugh, C. P. Johnson, and T. F. Tyler, "Reliability of shoulder range of motion comparing a goniometer to a digital level," *Physiotherapy Theory and Practice*, vol. 26, no. 5, pp. 327–333, 2010.

[15] A. Otten, C. Voort, A. Stienen, R. Aarts, E. van Asseldonk, and H. van der Kooij, "LIMPACT: An Hydraulically Powered Self-Aligning Upper Limb Exoskeleton," *IEEE Transactions on Mechatronics*, 2014 in press.

[16] J. Lenarčič and A. Umek, "Simple model of human arm reachable workspace," *Systems, Man and Cybernetics, IEEE Transactions on*, vol. 24, no. 8, pp. 1239–1246, 1994.

[17] N. Klopčar, M. Tomšič, and J. Lenarčič, "A kinematic model of the shoulder complex to evaluate the arm-reachable workspace," *Journal of biomechanics*, vol. 40, no. 1, pp. 86–91, 2007.

[18] C. A. Doorenbosch, J. Harlaar, and H. Veeger, "The globe system: An unambiguous description of shoulder positions in daily life movements," *Journal of Rehabilitation Research and Development*, vol. 40, pp. 147–156, 2003.

[19] S. J. Ball, I. E. Brown, and S. H. Scott, "MEDARM: a rehabilitation robot with 5dof at the shoulder complex," in *Advanced intelligent mechatronics, 2007 IEEE/ASME international conference on*. IEEE, 2007, pp. 1–6.

[20] C. Carignan, J. Tang, and S. Roderick, "Development of an exoskeleton haptic interface for virtual task training," in *Intelligent Robots and Systems, 2009. IROS 2009. IEEE/RSJ International Conference on*. IEEE, 2009, pp. 3697–3702.

[21] J. P. Snyder, *Map projections–A working manual*. USGPO, 1987, no. 1395.